Chapter 5

Growth and Characterization of Mixed Oxides (CuO-ZnO) Thin Films and Nano-particles

Starting from Zn doped CuO film (CZO) growth, formation of ZnO:CuO nano-composite and finally Cu doped ZnO thin films are prepared by dual target sputtering method, where the power of Zn target is systematically varied from 30W to 80W and Cu target is fixed at 18W. All Cu and Zn depositions were performed under O_2 plasma for the growth of Cu:Zn oxides (CZO). Afterwards, the as-deposited CZO films were then annealed at 400°C for 4hrs in air ambient. The structure, morphology, chemical and optical properties of the doped CZO thin films were investigated using various surface characterization techniques such as X-ray diffraction (XRD), scanning electron microscopy (SEM), X-ray photoemission spectroscopy (XPS) and Raman spectroscopy. For a very low concentration of Zn/(Cu) doping, the oxide films CuO/(ZnO) try to maintains their actual crystal structure with modified chemical and electronic properties. However, with increase in doping concentration, both oxide phases start to appear leading towards the formation of CZO based hetero-junction nano-composite. A similar kind of approach with chemical route has also been performed where lower Zn concentration results in formation of doped CuO nano-particle and with higher concentration a CuO-ZnO nano-composite. Finally, all XRD, SEM, Raman, UV-Vis and XPS results are in good correlation suggesting the formation of doped as well as CZO nano-composite with significantly different structures and properties.

5.1 INTRODUCTION

In earlier two chapters, we discussed the CO sensing mechanism of a p-type (CuO) and an n-type (ZnO) semiconductors, respectively. It has been observed that the oxidation process of both types has a great impact to their CO sensitivity as well as optimum operating temperatures. However, by successfully controlling the oxidation process of metal (Cu and Zn) films, it is possible to achieve a significantly high CO sensitivity for both oxides at a relatively lower operating temperature with fast response and recovery time. In addition, it is also capable to detect very low concentration of CO gas. Apart from these sensing parameters, another very important issue for any gas sensor is the selectivity of the sensor materials. In general, metal oxides are sensitive to many target gases as well as interfering gases. In this aspect ZnO would be a very good example as it can sense many gas and Volatile Organic Compounds (VOCs). This cross talk mechanism makes a gas sensor less selective to any particular target gas. Several efforts have been proposed as well as carried out to minimize the interference from ambient gases cross talk.

Some of the most promising approaches are either doping with noble or other metal nano-particles [1]. In addition, formation of MOs hetero-junctions as well as nano-composites would also be another effective approach. Both approaches can make a dramatic impact on enhancement of sensitivity as well as lowering the operating temperature. The dopant atoms and/or additives can effectively enhance the gas-sensing performance by altering the nanostructure surface morphology as well as energy band diagram. By systematically increasing the surface-to volume ratio and creating more and more interaction sites for target gas molecules on metal oxide active layer surface, gas sensitivity can be increased. At the same time, by varying the position of energy bands, surface interaction energy can be modulated to improve the selectivity issue of any sensor for a particular target gas or vapour.

Recently, a number of research works have been found based on the doping of transition metals within pure CuO nano-materials [2-4]. In the nano-scale range, CuO (nano-particles and thin films) shows the variable oxidation states such as $Cu^{0,}$ Cu^{+}, Cu^{2+}, where both type of doping (hole and electron carrier) is possible. It is a well known fact that the various dopants metals (Ni [5], Ce [6] and Zn [2]) can drastically modulate the electrical and optical properties of metal oxides (CuO). Among all metal dopants, Zn

would be one of the most compatible and promising candidate for CuO as Zn^{2+} is having almost similar ionic radii and ionic states of Cu^{2+} ions. This matching also makes Zn^{2+} ions thermodynamically more viable within the CuO host matrix [2]. Furthermore, for relatively lower Zn concentration, Zn atoms can easily occupy the Cu sites within the monoclinic structure of CuO without affecting its crystal property and Zn^{2+} dopants can also be produce as defects within CuO nano-structures [2].

Similarly, Cu doped ZnO would also be another effective approach to improve the CO sensing performance. Gong et al. reported that Cu doped ZnO nano-structures (Cu/Zn ratio = 0.38) significantly enhances the CO response as the surface resistance decreases with Cu concentration [7]. In addition, other metals were also used as dopant/additives to modify the gas sensing mechanism of the ZnO film surface. The effect of Al doping on ZnO nanostructures for gas sensing has also been reported [8 - 11]. It has been reported that the sensitivity of AZO film increases with reduction of film thickness [9]. Al doped ZnO nano-particles showed very high sensitivity for CO gas with a fast response for lower concentrations [11].

Apart from doping, hetero-junction nano-composite (mixed oxides) can also be very attractive for gas sensor and other device applications. ZnO-CeO_2 [12] and ZnO-SnO_2 [13] based mixed oxides are already reported for successful CO sensing. Similarly, CuO-SnO_2 based CO sensor has also been reported [14]. In addition to gas sensing application, CuO-ZnO mixed oxides based nanostructures are reported for photo-catalytic reduction of CO_2 [15]. This type of nano-composite is also found very much useful for solar energy harvesting [16].

Various growth techniques have been used to deposit/synthesize doped/composite metal oxides thin film / nano-particles. Among them, reactive DC sputtering [17], sol-gel [18], spray pyrolysis [19], and hydrothermal [20] methods are widely used. Within this chapter, we will discuss about the structure, morphology, chemistry and other analytical properties of doped and nano-composite Cu:Zn oxides with a special focus on nanostructures growth mechanism. Two different growth approaches have been used such as sputtering through the physical route where doping and hetero-junction nano-composites are formed. On the other hand, sol-gel method through chemical route is also employed for the growth of doped and composite nano-particles. Seven different Zn sputtering powers are used for the growth of CZO thin films

whereas four different Zn concentrations are used in chemical method to prepare the CZO nano-particles.

5.2 EXPERIMENTAL DETAILS

Zn doped CuO (denoted by CuO:Zn and vise versa ZnO:Cu) thin films were deposited on glass and silicon substrates at room temperature. In this physical growth route sputtering method was employed with dual metal targets of Cu and Zn. Ar plasma was used to sputter the metal atoms from the target electrodes whereas oxide is formed on substrate in presence of reactive O_2 gas. Prior to the deposition, substrates were ultrasonically cleaned using ethanol, acetone and iso-propanol in ex-situ and then dried under dry N_2 gas. During sputtered process, the concentration of Cu is fixed and the related power of Cu target (99.999% purity and 2-inch diameter) was fixed at 18W. While, the Zn concentration is varied by changing the sputtering power of the Zn target (99.999% purity and 2-inch diameter) in the range of 30W to 80W. During the deposition, the chamber pressure was remained ~1.84 $\times 10^{-2}$ mbar and the evaporation rate was controlled about ~ 0.7 - 1.1 Å/sec. To make a uniform deposition, the substrates were rotated at a low speed of ~10 rpm and homogeneous thin films are formed. Afterwards, CuO:Zn thin films were thermally annealed at 250°C for 3hrs within the deposition unit in presence of argon (Ar) gas (11.5 sccm). Afterwards, the samples are further ex situ oxidized in air ambient (muffle furnace) at 400°C for 4hrs. A slow cooling rate (10°C/ min) was preferred to minimize the possible thermal stress and improve crystalline quality of the films.

On the other hand, a simple chemical route (sol-gel) is used to synthesis the Zn doped CuO nano-particles and CZO based nano-composites. All the chemicals used in this experiments such as copper acetate monohydrate (Cu $(CH_3CO_2)_2 \cdot 2H_2O$), Urea (CO $(NH_2)_2$) and zinc acetate monohydrate (Zn $(CH_3CO_2)_2 \cdot 2H_2O$) are commercially purchased. Copper acetate monohydrate is used as the starting material, while zinc acetate monohydrate is used as a solvent and urea is used as a stabilizer for the preparation of Zn doped CuO nano-particles. The solution is prepared from a 0.94M solution of copper acetate monohydrate and 1M of urea dissolved into 2ml, and 12ml of DI (de-ionized) water, respectively. Afterwards, a 0.04M, 0.06M and 0.08M of zinc acetate monohydrate was added into the as-prepared solution for varying the

concentration of ZnO. For a complete dissolution, the mixture is stirred on hot plate at 80^{o}C temperature for 5 hours. Afterwards, the solution is put on oven at 150^{o}C temperature for 4 hours in air ambient to evaporate the excess solvent. Finally, dark grey colored gel is collected and then annealed the gel at 400^{o}C temperature in air for 3hours.

All doped Zn / (Cu) metal oxides CuO / (ZnO) thin films/nano-particles as well as CZO nano-composites were characterized for structural, morphological, optical and chemical properties using various analytical techniques such as XRD, FESEM, Raman spectroscopy, UV-vis spectroscopy and XPS. These techniques have also been used to find the effect of doping on their structural, optical and chemical properties of Zn doped CuO thin films/nano-particles.

5.3 RESULTS AND DISCUSSION

Various characterization techniques such as X-ray diffraction (XRD), scanning electron microscope (SEM), UV-vis spectroscopy, Raman spectroscopy and X-ray photoelectron spectroscopy (XPS) has been used for the studies of structural properties, surface morphology, optical properties and chemical properties, respectively. Finally, a correlation between various characterizations is also discussed.

5.2.1 X-ray Diffraction (XRD)

Pure cupric oxide (CuO) thin film, prepared at 400°C for 4hrs in air ambient is denoted as Sample 01. The sputter target power of Zn metal is varied from 30W to 80W for Zn doped CuO thin films and named as Sample 02 to Sample 07, respectively. Figure 5.1 shows the XRD patterns of CuO thin films with variable Zn contents. Scan range of 2θ is shown between 30^{o} and 50^{o} and all CuO and ZnO diffraction peaks are marked. The XRD peak positions are consistent with the pure CuO and ZnO crystal lattices. As discussed in chapter 3, pure CuO films appear with (111) and (-111) diffraction lines of monoclinic phase positioned at 2θ = 35.5° and 38.8°, respectively [Figure 5.1 (a)]. It is clearly noticed that only CuO peaks are present in XRD spectra for Zn target power up to 40W, [Figure 5.1(b) and (c)]. Sharp peaks with high intensity indicated the crystalline nature of the samples. Although, there is no trace of any ZnO diffraction peak for Sample 2 and Sample 3, however, a significant difference in XRD pattern is also observed. The (111) diffraction peak of pure CuO is not visible for these doped oxide films. This

finding indicates that Zn atoms are mostly following the Cu lattice positions of CuO and behave like a dopant material [21]. Hence, Zn ions are successfully doped at the Cu sites without affecting the structure of the parent CuO crystal.

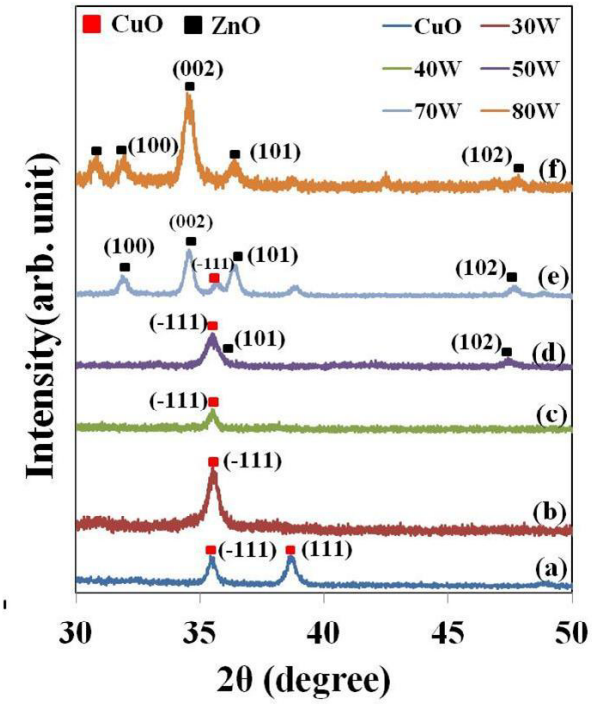

***Figure 5.1**: XRD patterns of pure and doped CuO thin films with different concentration of Zn, thermally oxidized at 400^{o}C for 4hrs in air ambient.*

With increase in Zn target power to 50W, the concentration of Zn significantly increases. As a result, additional diffraction peaks of ZnO (102) crystal plane at 47.8° starts to appear along with the existing CuO (-1 1 1) diffraction line as shown in Figure 5.1 (d) [22-24]. This additional ZnO peak confirms the presence of both metal oxides (CuO and ZnO) and hence the formation of nano-composite. With further increases in Zn power, the intensity of ZnO diffraction peaks become more and more stronger, at the cost of CuO peaks. The increase of Zn dopant would also affect the concentrations of the interstitial Zn, oxygen vacancies and Cu vacancies [25-27]. Further increase in Zn power to 70W (Sample 06) makes a drastic change in XRD pattern. Mostly ZnO related peaks (2θ = 31.92, 34.66, 35.15, 38.83 and 47.74) are found with relatively higher intensities. All these well-defined diffraction peaks are in good agreement with earlier reported values of ZnO diffraction peak positions [18 -20]. This finding suggests that ZnO is the turned as the major oxides phase within the film with a minor fraction of CuO clusters,

as can be seen in Figure 5.1 (e). For a Zn power of 80W, CuO diffraction peaks are completely disappeared. This finding can be explained as Cu doped ZnO film formation, where the Cu atoms are incorporated within the ZnO crystal lattice [Figure 5.1 (f)].

The XRD results of chemically grown nano-particles are very different as compared to that of sputter samples. In general, it appears with many diffraction peaks due the all possible orientation of the nano-particles. The XRD patterns of Zn doped CuO nano-particles with different molecular wt% of Zn (0.04M, 0.06M and 0.08M) are shown in Figure 5.2. Pure CuO nano-particles show sharp peaks at the position of 2θ = 32.44°, 35.26°, 38.42°, 48.60°, 53.32°, 57.96°, 61.08°, 65.44° and 67.24° correlated to (110), (-111), (111), (-202), (020), (202), (-113), (-311) and (113) planes of CuO, respectively [25]. These observed peaks suggested a single oxide phase CuO with a monoclinic structure is formed [26; JCPDS cards no.: 89-2529]. This diffraction peaks appear quite similar for Zn concentrations of 0.04M and 0.06M, which suggest that the crystallinity of CuO nano-particles is still maintain and Zn occupies the defect sites as a dopant material. However, an additional peak of ZnO is observed at 2θ = 35.15° in the XRD for further increase of Zn concentration to 0.08M. This peaks is assigned as the (101) plane of ZnO, as shown in Figure 5.2 (d). This peak intensity and position gives a strong indication of ZnO cluster formation within the CuO film. Hence, we can conclude that it is the initial stage of hetero-junction nano-composite formation. Further increase in Zn concentration onwards will result in relative increase of ZnO phase within the CuO layer. In any case, the (-1 1 1) and (111) diffraction peaks of CuO are found most intense for all doped samples. In principle, the peak intensity is determined by the nature of the atom and perhaps the available atoms in a particular crystal plane. Similarly, if the associated atoms in a diffracting plane of a unit cell are different or if the atoms in a particular plane are strained or compressed (depends on the size of the dopant atom) due to the dopant foreign impurity atom, the peak shape and intensity will be different for that particular plane. Another possible reason for the higher peak intensities for (-111) and (111) CuO plane may be a lower surface free energy which influences a preferential growth of these planes. Due to this anisotropy, preferential growth on the plane of lowest energy occurs and is accounted for the observed larger intensity of the diffraction peaks in the XRD pattern [26 -27]. No extra impurity peaks of ZnO) are detected in XRD below 0.08M, indicating the doping limit of the Zn within CuO lattice. Hence, up to 0.06M, Zn does not affect the crystal structure of CuO nano-particles.

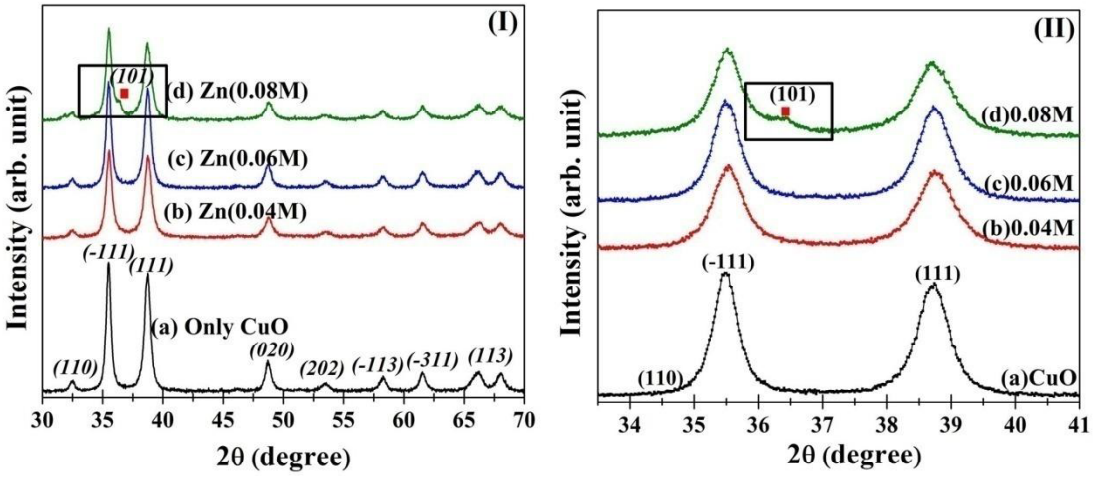

***Figure 5.2**: XRD patterns of (a) pure CuO nano-particles and Zn doped (b) 0.04M, (c) 0.06M, (d) 0.08M of CuO nano-particles.*

In the case of highly doped (0.08M) CuO nano-particles, the preferential orientation of (111) plane of CuO nano-particle becomes slightly wider and an additional peak appear which we assigned as (101) plane of ZnO phase [Figure 5.2 (d)]. For better understanding, a closer view of the XRD spectra are also compared as shown in [Figure 5.2 (II)]. A small change is observed in 0.08M doped CuO nano-particles as compared to the pure CuO nano-particles. The (101) ZnO diffraction peak gets intense with further increase in Zn concentration. The absence of ZnO diffraction peaks for lower Zn concentration can be explained in the following way. Zn ions can successfully replace the Cu ions into CuO crystal due to the similarity in the ionic radii of Cu (0.72 A) and Zn (0.74 A). Hence, only CuO diffraction lines can be seen in the XRD patterns of the doped CuO samples [28]. Therefore, the absence of ZnO peaks in the XRD patterns for the synthesized nano-particles below 0.06M of Zn precursor confirms the successful substitution of Zn ion on the Cu ions sites in CuO lattice [28].

The micro-structural parameters such as average crystallite size (D), dislocation and micro-strain (ε) for all deposited/synthesized thin films/nano-particles have been estimated using the "*Scherrer formula"* [29].

$$D = (0.91\,\lambda) / (\beta\,Cos\theta)$$

Where λ is the wave length of X-ray (0.1541 nm), β is the full width at half maximum (FWHM) in radian, θ is the diffraction angle and D is the particle diameter [30]. The average crystallite size (D) of CuO has been found to increase with the increasing

concentration of Zn (power of Zn target), while micro-strain (ε) is found to decrease as shown in Figure 5.3. This behavior may be attributed to the slightly larger ionic radii of dopant Zn ions as compared to host Cu ions [31-32]. Moreover, composite formation can also reduce the internal compressive stress by segregating individual oxide phases through domain boundary formation.

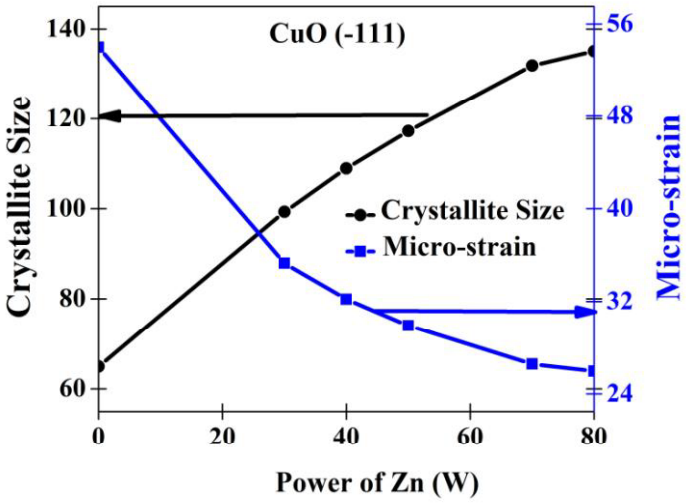

***Figure 5.3**: Variation in Crystallite size (D) and micro-strain (ε) of CuO thin films as a function of Zn dopant concentration (power of Zn target).*

5.2.2 Scanning Electron Microscopy (SEM)

In general, the surface morphology of the oxide thin-films / nano-particles strongly depend upon many parameters such as growth process, oxygen partial pressure, films thickness, oxidation temperature, dopant concentration etc. Among these, growth process can drastically modify the surface texture of the oxide layer even in nano-scale. It can also be very sensitive to the dopant (Zn) concentration. Here, we discuss the influence of Zn concentration on the surface morphology of CuO thin films and nano-particles, using FESEM results.

In case of reactive sputter deposited oxide thin films, a comparison of the surface morphologies of Zn-doped CuO, CuO-ZnO nano-composite and Cu-doped ZnO film have been depicted in Figure 5.4. The morphology of the pure CuO film surface appears very different from the earlier CuO thin films prepared from vacuum deposition of Cu film followed by thermal oxidation (discussed in Chapter 03). This can be related to the growth process as CuO thin films are prepared here using reactive sputtering. A typical

SEM image of CuO thin film on glass substrate is shown in Figure 5.4 (a), whereas Figure 5.4 (b) shows a closer look of it. The surface appears with large flat-top islands uniformly distributer over the continuous layer. The flat island's top suggests layerd growth morphology is preferable for this growth condition.

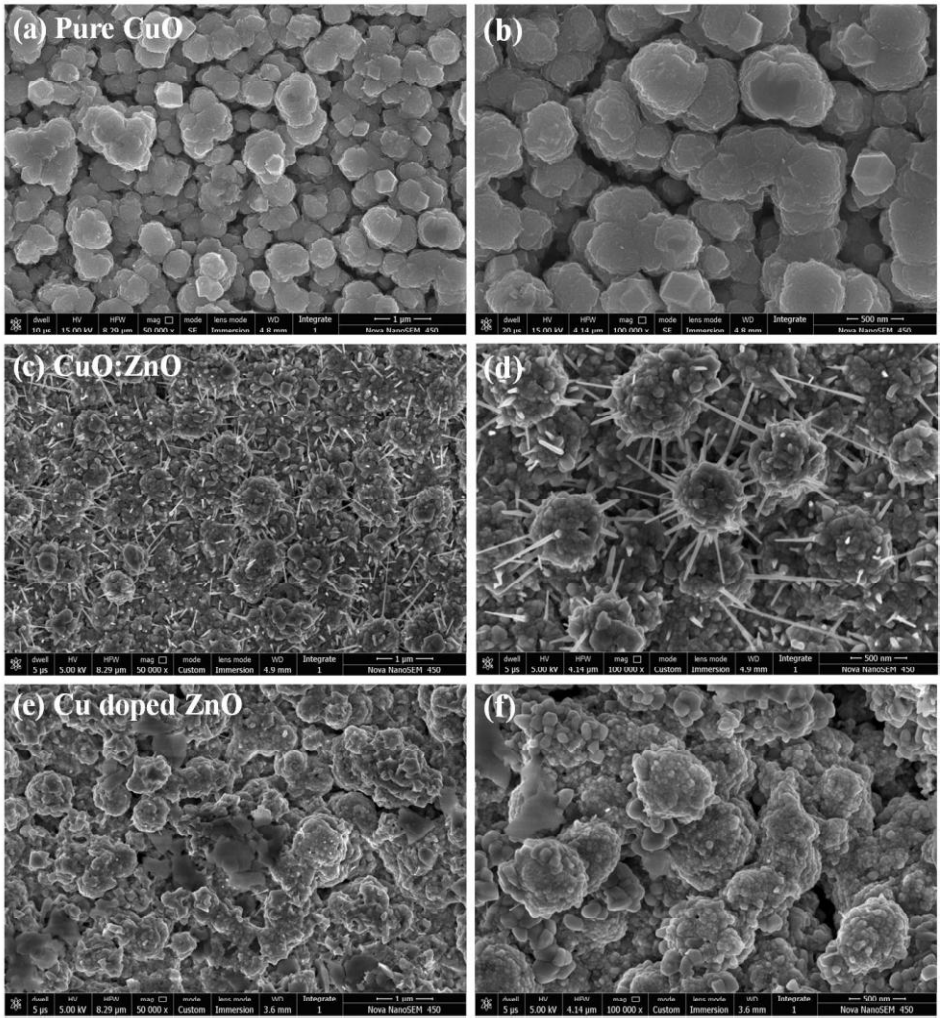

***Figure 5.4**: FESEM results of (a) pure and doped CuO_x thin films with different concentration of Zn (b) Zn@50W, (c) Zn@80W, deposited using sputtering method and then thermally oxidized at 400^oC for 4hrs on glass substrate.*

However, for Zn-doped CuO films (Zn target power up to 40W), the morphology does not change significantly, apart from a mild surface roughening which can be related to a reduced surface diffusion CuO species in presence of Zn dopant, promoting a vertical growth. An interesting surface morphology is found as the Zn concentration is further increased (Zn@50W), where ZnO-CuO nano-composites are expected to form [Figure 5.4 (c) and (d)]. The overall surface appears with similar type of large islands

structure which are almost connected together on the base and decorated with many spiky nano-rods randomly orientation over it. The flat-top islands turn to cauliflower-like structure due to the surface roughening and 3D growth of CuO. It is assumed that the asymmetric growth is mostly driven by the ZnO nano-rods formation. These findings are in good agreement with earlier XRD results which also suggest a nano-composite formation rather than simple Zn doping within the CuO film. In case of Zn power above 70W, the SEM image appears very different. The nano-rods are not visible any more. Granular structures are formed on the cauliflower-like base islands. Figure 5.4 (e) and (f) show the surface morphology of a film with 80W Zn power. We assume this as formation of Cu-doped ZnO film, as discussed in XRD.

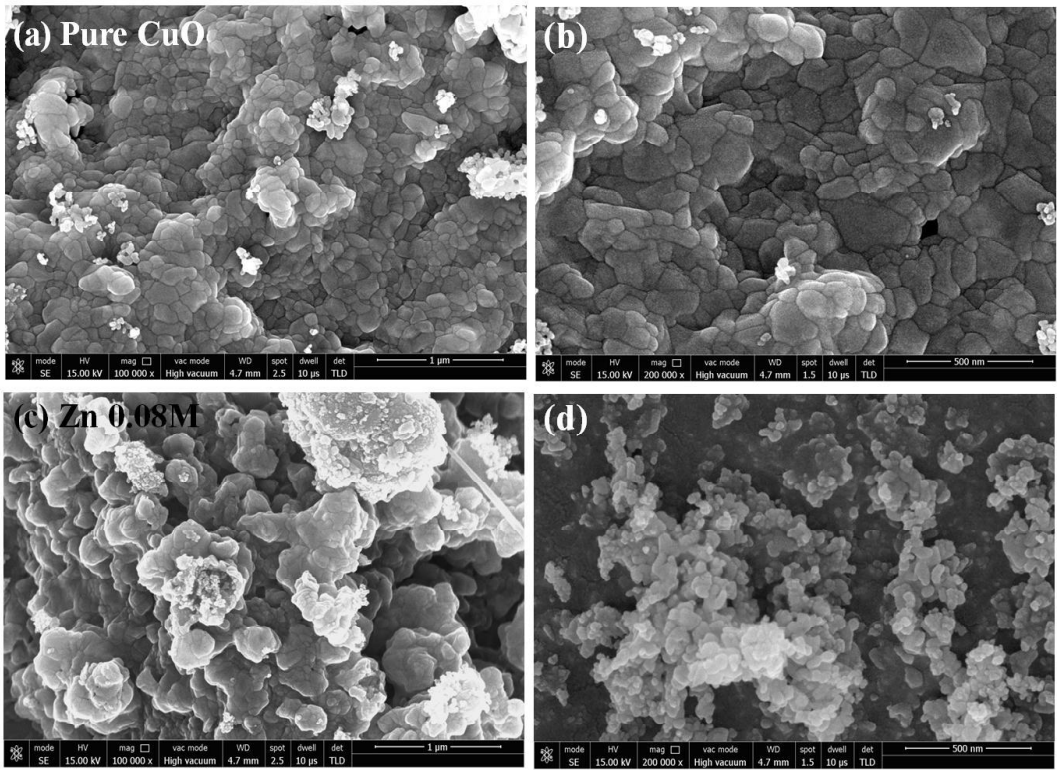

Figure 5.5: *FESEM results of (a) pure CuO nano-particles (b)CuO-ZnO nano-composite with 0.08M concentration of Zn.*

Chemically synthesized pure and Zn doped CuO nano-particle's surface are depicted in Figure 5.5. As compared to earlier films, pure CuO surface appears with structures [Figure 5.5 (a) and (b)]. However, with addition of Zn dopant, a surface roughening is observed. Figure 5.5 (c) and (d) represent the nano-particle surface with Zn precursor concentration of 0.08M. Very tiny flake-like structures are found on top of

the large granular islands. As it is expected to be a formation of nano-composite of CuO-ZnO with CuO as the majority of oxide film, we can assume that the tiny flake-like structures are mainly of ZnO whereas the granular islands are formed with CuO.

5.3.3 UV-vis spectroscopy

Optical absorption spectra of chemically synthesized CuO nano-particles with different Zn dopant concentrations have been investigated using UV-visible spectrophotometer at room temperature (RT), within a wavelength range of 200-900 cm^{-1}. This spectroscopy is further used to estimate the optical band-gap of the nano-particles and also see the effect of Zn dopant. UV-visible absorption spectra of pure and Zn-doped CuO nano-particles and the corresponding band-gap are shown in Figure 5.6. The UV-visible absorption spectra of pure and various Zn-doped CuO nano-particles are shown in Figure 5.6 (a) [26, 33]. The UV-visible spectra of pure (un-doped) CuO nano-particles exhibit a strong absorption peak at 265nm, which is red shifted with the increase of Zn doping concentration [26, 34]. In addition, increasing in dopant concentration also results in broadening of the absorption peak towards the visible region. It is observed from Figure 5.6 (I) that Zn doping has improved the visible light absorption capability of CuO nano-particles. This enhancement of absorption in visible light region with Zn doping may be attributed to d-d transition between closely spaced Zn^{2+} and Cu^{2+}ions [35]. Moreover, it can also be related to the wider band gap of ZnO as compared to CuO. Therefore, these doped CuO can be more promising for visible light photo-catalytic activity as well as solar cell applications.

The energy band gap (E_g) of the Zn-doped nano-particles is calculated using "Tauc Relation" as given below [26]:

$$(\alpha h\nu) = A\,(h\nu - E_g)^n$$

where, A is a constant, which depends on the electron transition probability (n = ½, direct allowed transition), E_g is the band gap energy (eV), h is the Plank constant (6.627×10^{-34} J.sec) and ν is the frequency. Hence, the "Tauc equation" is follows as [26]:

$$(\alpha h\nu)^2 = (h\nu - E_g) \text{ and } h\nu = hc/\lambda = 1240/\lambda)$$

where, α is the absorption coefficient and λis the wavelength of the light. The absorption coefficient can be further expressed as follows using [26]:

$$\alpha = 2.303 \log (T/d)$$

where, d is the thickness of thin films and T is the transmission.

Figure 5.6 (II) shows the Tauc plot $(\alpha h\upsilon)^2$ *vs.* $h\upsilon$ of pure and Zn doped CuO. The energy band gap for these nano-particles can be estimated from the intercept of the extrapolation of the liner region of $(\alpha h\upsilon)^2$ vs. $h\upsilon$ as shown with dotted lines. A gradual increase in direct energy band gap starting from 1.75 for pure CuO to 2.00 eV for Zn-doped CuO films is found here. The Tauc lot for the ZnO-CuO nano-composite (0.08M) is shown in Figure 5.6 (III) where an energy band gap is drastically increased to 3.6 eV. This finding is in good agreement with the band gap of ZnO and hence further confirms the formation of ZnO phase within the CuO layer. Figure 5.6 (IV) represents the band gap energy of the Zn:CuO nano-particles as a function of Zn precursor concentration.

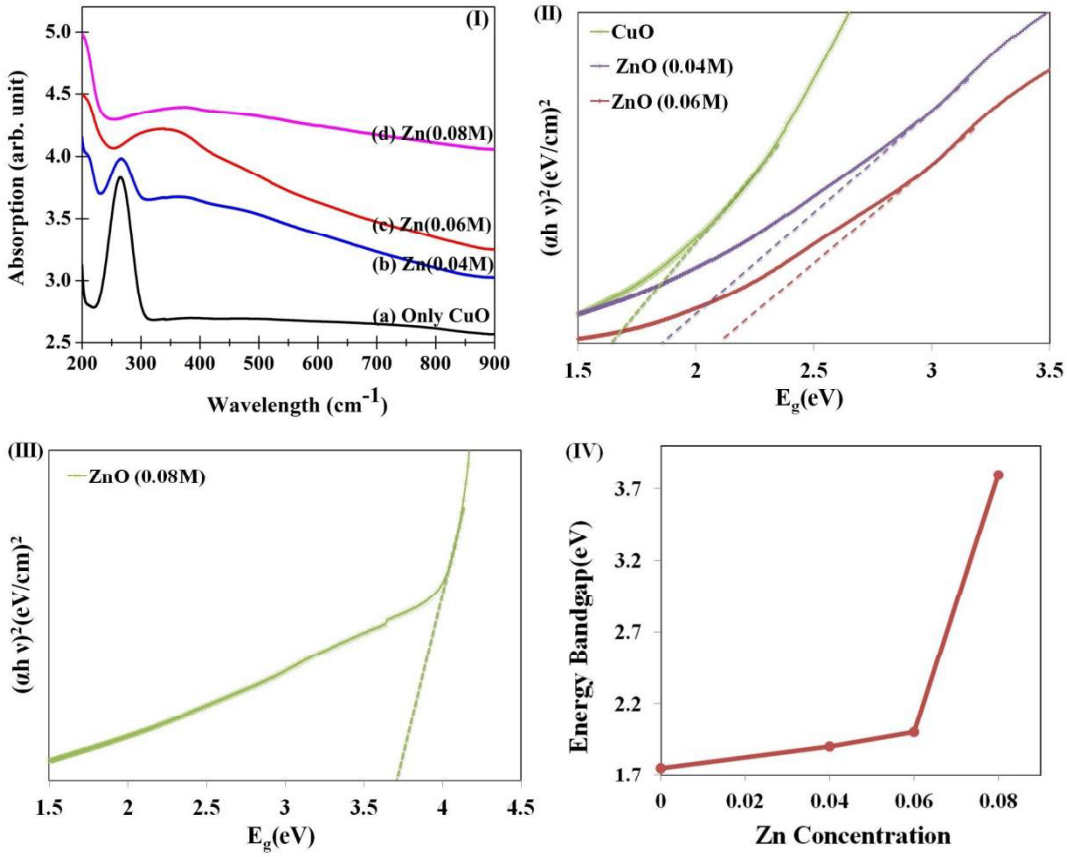

Figure 5.6: *(I) UV-visible absorption spectra, Tauc $[(\alpha h\upsilon)^2$ vs. $h\upsilon]$ plots for (II) Zn-doped CuO and (III) CZO nano-composite and (IV) variation of the band gap with Zn concentration of pure and Zn doped CuO nano-particles.*

5.3.4 Raman Spectroscopy

Raman spectroscopy has been used to investigate the Zn doping mechanism with the CuO films and nano-particles. For proper oxidation and homogeneous mixing, all Zn doped CuO thin films are annealed at 400°C for 4hrs in air ambient. Figure 5.7 represents the Raman spectra of reactive sputter grown oxide samples for different Zn target power. Figure 5.7 (a) displays the Raman spectra of pure CuO films (Sample 1). The significant Raman peaks at 292, 341 and 626 cm^{-1} can be identified as the first order A_g and $2B_g$ phonon scattering of CuO [36]. Details of these are already discussed in Chapter 03 for thermally oxidized thin Cu film. Similar type of results are also observed for doped Sample 2 (Zn@ 30W) as shown in Figure 5.3(b), however, a minor trace of ZnO can also be seen in Sample 3 (Zn@ 40W). In case of ZnO-CuO nano-composites (Sample 4 (Zn@ 50W) and Sample 5 (Zn@60)) Raman spectra appear with both CuO and ZnO peaks as shown in Figure 5.7(c). The main peak of ZnO is observed at around 438.7 cm^{-1} and another spectra position are at 563.6 cm^{-1} and 554.7 cm^{-1}.

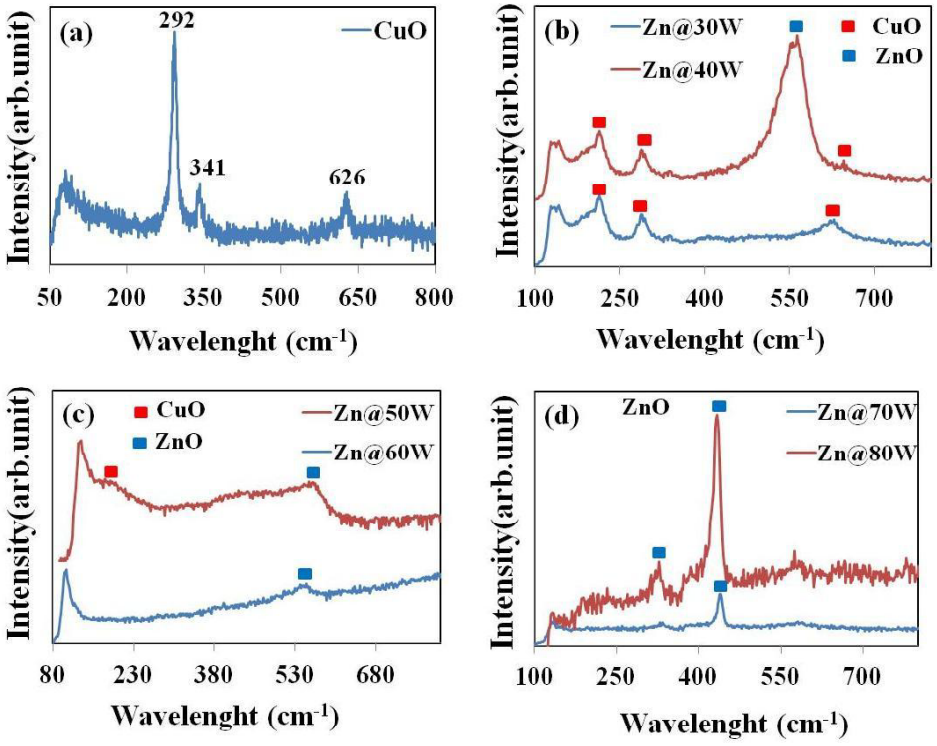

***Figure 5.7**: Raman spectra of (a) pure and doped CuO_x thin films with the power of Zn target are (b) 30W and 40W, (c) 50W and 60W, (d) 70Wand 80W.*

It is quite clear from the observed Raman spectra that with increase in Zn target power, the peak intensity of ZnO increases at the cost of CuO peak intensities. In the case of Sample 6 and sample 7 (Zn target power 70W and 80W) the A_g mode of CuO is almost vanished and a strong peak at 439 cm^{-1} originated from the ZnO E2 mode appears [Figure 5.7(d)]. These finding are very much complementary with our XRD and SEM results, suggesting Zn doped CuO formation up to Zn target power of 40W and Cu-doped ZnO formation above 70W. In between it appears with a composite of ZnO-CuO [39].

Raman studies of chemically grown CuO nano-particles with different Zn-dopping are shown in Figure 5.8. Similar to physically deposited films, pure CuO film appears with Raman peaks at 292, 341, 626 and 1090 cm^{-1}. With increase of Zn precursor concentration, CuO peaks are getting relatively weaker and at about 0.08M, additional peak attributed to ZnO is appeared [Figure 5.8]. This finding is very much in line with the XRD and UV-vis results, suggesting the CuO-ZnO composite formation starts at 0.08M of Zn precursor concentration.

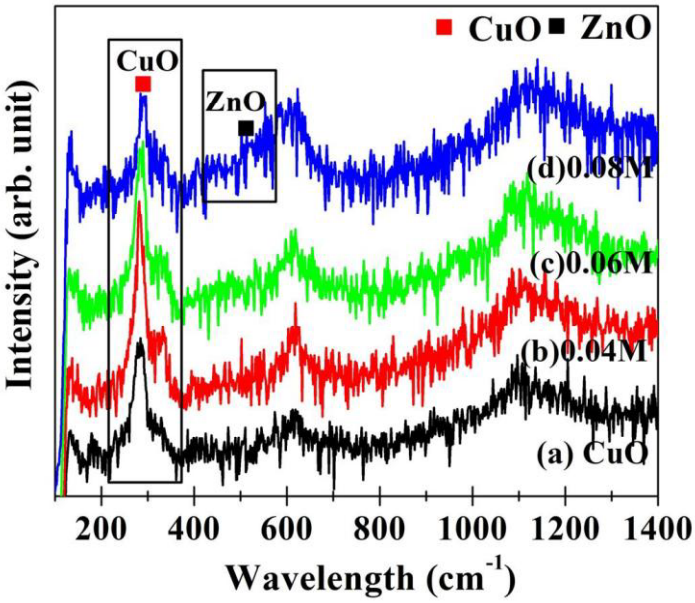

***Figure 5.8**: Raman spectra of (a) pure and doped CuO_x nano-particles (b) 0.04M, (c) 0.06M and (d) 0.08M).*

5.3.5 X-ray photoelectron spectrometry (XPS)

X-ray photoemission spectroscopy (XPS) measurement was performed for a qualitative analysis of the sputtered grown Zn:CuO samples. As X-ray source, both

monochromatic (1486.6 eV) and Mg K_α (1256.7 eV) lines were used here. Figure 5.9 shows the survey scans of doped oxide films for Zn power below 40W and above 70W. In this study, the top few 10nm of the film was removed under UHV for cleaning purpose and Al K_α line was used as X-ray source. Different core binding energies along with Auger peaks are clearly assigned. It is quite clear from Figure 5.9 that below 40W of Zn power sample is mostly of CuO type whereas above 70W it shows ZnO type properties. Both 30W and 40W samples does not show any Zn2p peaks and appear with very strong Cu2p peaks indicating its CuO nature. At the same time, 70W and 80W sample appear with Zn2p lines without having Cu2p, suggesting its dominating ZnO nature. These finding are in good agreement with earlier analysis where we conclude that below 40W Zn-doped CuO film is formed and above 70W it is of Cu-doped ZnO film.

To investigate the CuO-ZnO composite films, XPS results of 60W sample is also compared with others as shown in Figure 5.10. In this case, samples were thermally out-gassed under UHV for cleaning purpose and MgK_α line was used as X-ray source. Survey spectra appear with different core level and Auger binding energy peaks as marked in Figure 5.10(a). Core level BE spectra are very similar to earlier results but Auger lines have a shift of about 230eV as the X-ray source is changes. Most interestingly, survey scan of 60W sample clearly shows both Cu2p and Zn2p BE lines, indicating a well balance between both metal contents. It is also well matching with our conclusion of ZnO-CuO composite formation for this sample.

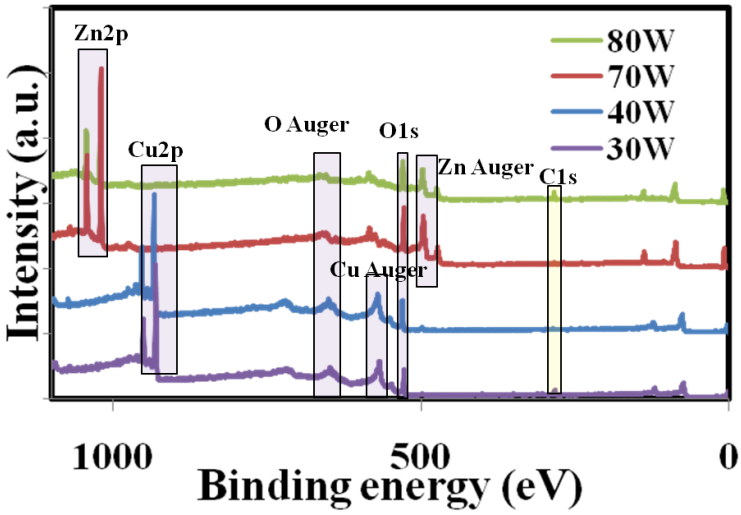

***Figure 5.9**: XPS survey scans sputter grown doped Zn:CuO films with various Zn concentrations* (*using Al-K_α* line).

To confirm the presence of the dopant atoms within the host oxide crystals, high resolution scans of Cu2p and Zn2p BE spectra of 60W sample are compared with 40W and 70W samples [Figure 5.10(b) and (c)]. Although, survey scan does not show the presence of Zn2p line for 40W sample, however, high resolution scan with longer accusation time clears this doubt as shown in Figure 5.10(b). Similarly, 70W sample also appear with a weak Cu2p line in high resolution scan [Figure 5.10(c)]. Both these spectra clearly establish the presence of dopants within the host oxides whereas XRD and SEM results confirm their host oxide crystal structures and morphologies.

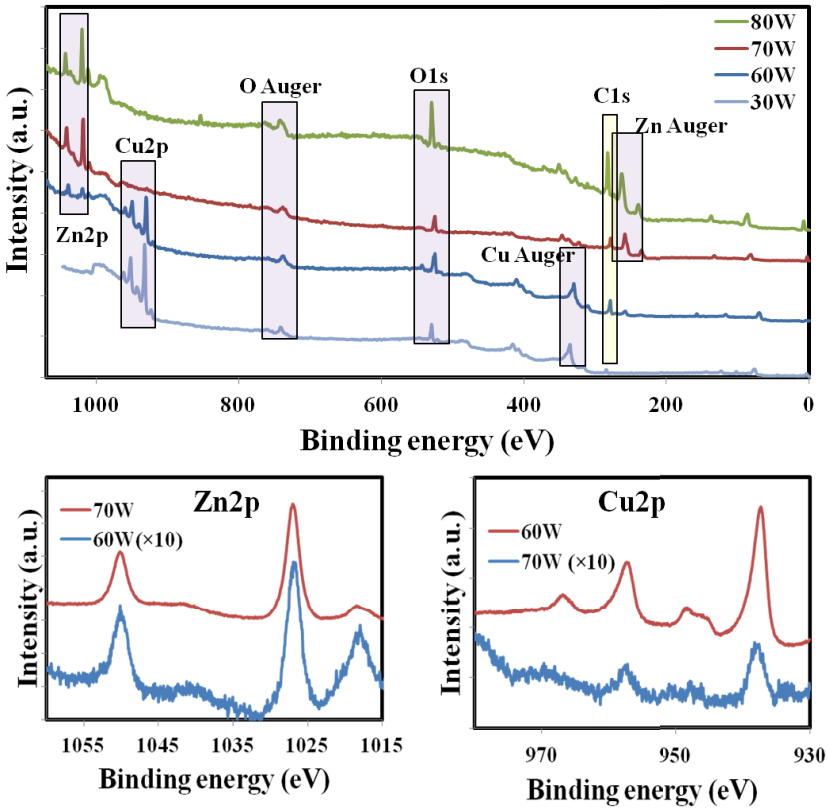

***Figure 5.10**: XPS survey scans sputter grown doped Zn:CuO films with various Zn concentrations* (*using Mg-K_α* line).

The overall summary of the mixed oxide formation is schematically represented with bar graph in Figure 5.11. Different phases of mixed ZnO:CuO are shown with bar graph for both physical and chemical growth routes. Figure 5.11(a) represents the sputter grown mixed oxide phases where Zn target power of 40W and 70W represents the boundaries between Zn-doped CuO to ZnO:CuO nano-composite and ZnO:CuO nano-composite to Cu-doped ZnO formations, respectively. Similarly, Figure 5.11(b) appears for chemical synthesis of mixed oxide through sol-gel method where Zn pre-cursor concentration of

0.07M represents the boundary between Zn-doped CuO to ZnO:CuO nano-composite formation.

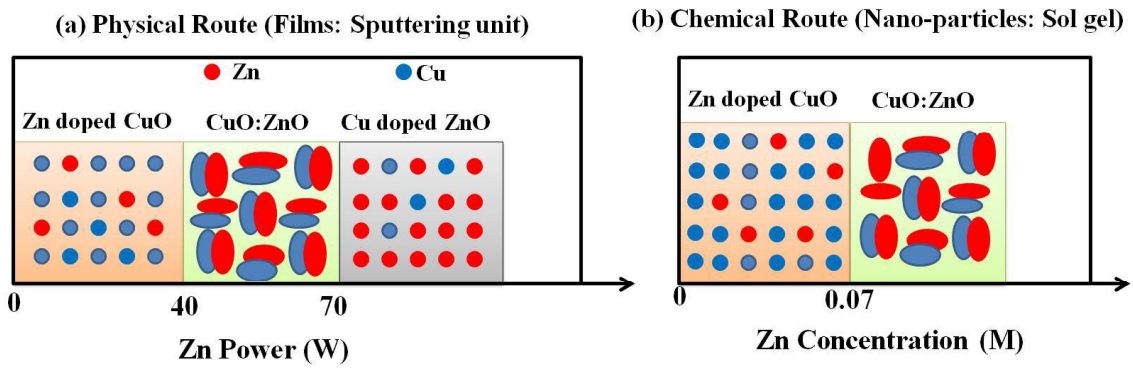

***Figure 5.11**: A schematic of the bar graph for different phases of ZnO:CuO mixed oxides (a) Physical growth route through sputter deposition and (b) Chemical growth route through sol-gel synthesis.*

5.4 SUMMARY

A systematic study of the doping mechanism and nano-composite formation for CuO: ZnO thin films and nano-particles system has been investigated for structural, morphological, chemical and optical properties. Two different growth processes such as sputtering and sol-gel methods have been employed. For sputter method, Zn-doped CuO films are formed up to a Zn target power of 40W and afterwards CuO-ZnO nano-composite starts to form. Finally, Cu-doped ZnO are happened to form above Zn power of 70W. Usually, doped samples appear with granular islands structure whereas for nano-composite, nano-rods are found on top these granular islands. For sol-gel growth process, Zn-doped CuO nano-particles are formed up to a Zn precursor concentration of 0.06M. For 0.08M concentration, composite of ZnO-CuO starts to form as schematically presented in Figure 5.11(b). The optical energy band gap for composite structure drastically increased from 1.8eV to about 3.6eV. Finally, these doped and composite nanostructures are expected to be very much useful for various catalytic and sensor applications.

Bibliography

[1] D. Kohl, Sensors Actuators B 1 (1990) 158.

[2] J. Iqbal, T. Jan, S. U. Hassan, I. Ahmed, Q. Mansoor, M. U. Ali, F. Abbas and M. Ismail, AIP Advances 5 (2015) 127112.

[3] J. Jayaprakash, N. Srinivasan, P. Chandrasekaran and E. K. Girija, Molecular and Biomolecular Spectroscopy 136 (2015) 1803.

[4] P. Bandyopadhyay, A. Dey, R. Basu, S. Das and P. Nandy, Current Applied Physics 14 (2014) 1149.

[5] S. A. Amri, M. S. Ansari, S. Rafique, M. Aldhahri, S. Rahimuddin, A. Azam and A. Memic, Current Nanoscience 11 (2015) 191.

[6] T. Jan, J. Iqbal, Q. Mansoor, M. Ismail, S. H. Naqvi, A. Gul, S.F.H. Naqvi and F. Abbas, Journal of Physics D: Applied Physics 47 (2014) 355301.

[7] H. Gong, J. Q. Hu, J. H. Wang, C. H. Ong and F. R. Zhu, Sensors Actuators B Chemistry 115 (2006) 247.

[8] S. C. Navale, V. Ravi, I. S. Mulla, S. W. Gosavi and S. K. Kulkarni, Sensors Actuators B 126 (2007) 382.

[9] J. F. Chang, H. H. Kuo, I. C. Leu and M. H. Hon, Sensors Actuators B 84 (2002) 258.

[10] Z. Yang, Y. Huang, G. Chen, Z. Guo, S. Cheng and S. Huang, Sensors Actuators B 140 (2009) 549.

[11] M. Hjiri, L. E. Mir, S. G. Leonardi, A. Pistone, L. Mavilia and G. Neri, Sensors Actuators B Chem. 196 (2014) 413.

[12] M. F A. Kuhaili, S. M. A. Durrani and I. A. Bakhtiari, Applied Surface Science 255 (2008) 3033.

[13] E. Nikan,A. A. Khodadadi and Y. Mortazavi, Sensors Actuators B Chem. 184 (2013) 196.

[14] J. H. Jeun, D. H. Kim and S. H. Hong, Materials Letters 105 (2013) 58.

[15] W. N. Wang, F. Wu, Y. Myung, D. M. Niedzwiedzki, H. Soon Im, J. Park, P. Banerjee and P. Biswas, ACS Applied Materials & Interfaces 7 (2015) 5685.

[16] Fei Wu, "Copper and Zinc Oxide Composite Nanostructures for Solar Energy Harvesting" PhD thesis, Washington University in St. Louis, Engineering and Applied Science (2015).

[17] F. H. Wang, J.C. Chao, H. W. Liu and T. K. Kang, Journal of Nanomaterials 936482, (2015) 1.

[18] C. Zegadi, K. Abdelkebir, D. Chaumont, M. Adnane and S. Hamzaoui, Advances in Materials Physics and Chemistry 4 (2014) 93.

[19] R. Biswa, A. Maldonado, J. V. Perez, D. R. Acosta and M. D. L. L. Olvera, Materials 7 (2014) 5038.

[20] A. Zainelabdin, G. Amin, S. Zaman, O. Nur, J. Lu, L. Hultmanb and M. Willander, Journal of Materials Chemistry 22 (2012) 11583.

[21] S. Choudhary, J. V. N. Sarma and S. Gangopadhyay, AIP Conference Procedings 1724 (2015) 020116.

[22] S. G. Rejitha and C. Krishnan, Sciencia Acta Xaveriana, "An International Science Journal 4 (2013) 91.

[23] I. Mihailova, V. Gerbreders, E. Tamanis, E. Sledevskis, R. Viter and P. Sarajevs Journal of Non-Crystalline Solids 377 (2013) 212.

[24] S. Choudhary and S. Gangopadhyay, AIP Conference Proceedings 1989 (2018) 020007.

[25] T. T. Minh, N. T. T. Tu, T. T. V. Thi, L. T. Hoa, H. T. Long, N. H. Phong, T. L. Minh Pham and D. Q. Khieu, Journal of Nanomaterials 5198045 (2019) 1.

[26] T. Shahid, M. Arfan, W. Ahmad, T. BiB, and T. M. Khan, Advance Materials Letters 7 **(**2016) 100.

[27] N. Fujimura, T. Nishihara, S. Goto, J. Xu and T. Ito, Journal of Crystal Growth 130 (1993) 269.

[28] V. Figueiredo, E. Elangovan, G. Goncalves, P. Barqunha, L. Pereira, N. Franco, E. Alves, R. Martins and E. Fortunato, Appl. Surf. Sci. 254 (2008) 3949.

[29] H. M. Cakmak, H. A. Cetinkara and S. Kahraman, Super Lattices and Microstructures 51 (2012) 421.

[30] J. D. Aiken and R. G. Finke, Journal of Molecular Catalysis A Chemistry 145 (1999) 1.

[31] T. Shahid, M. Arfan, W. Ahmad, T. BiBi and T. M. Khan, Advanced Materials Letters 7 (2016) 100.

[32] J. Iqbal, T. Jan, S. U. Hassan, I. Ahmed, Q. Mansoor, M. U. Ali, F. Abbas and M. Ismail, AIP Advances 5 (2015) 127112.

[33] S. Krishnan, A. S. M. A. Haseeb and M. R. Johan, Journal Alloys Compounds 586 (2014) 586.

[34] J. Wang, S. He, Z. Li, X. Jing and M. Zhang, Colloid Polymers Science 287 (2009) 853.

[35] M. T. Qamar, M. Aslam, I. M. I. Ismail, N. Salah, and A. Hameed, ACS Applied Materials Interfaces 29 (2015) 8757.

[36] S. Choudhary, J. V. N. Sarma, S. Pande, S. A. Girard, P. Turban, B. Lepine and S. Gangopadhyay, AIP Advance 8 (2018) 055114.

[37] S. Meti, M. R. Rahman, Md. I. Ahmad and K. U. Bhat, Applied Surface Science 451 (2018) 67.